INFRARED MICROSPECTROSCOPIC CHEMICAL IMAGING APPLIED TO INDIVIDUAL STARCH GRANULES AND STARCH DOMINANT SOLID MIXTURES

by

MARK DANIEL BOATWRIGHT

B.S., Kansas State University, 2009

A THESIS

submitted in partial fulfillment of the requirements for the degree

MASTER OF SCIENCE

Department of Grain Science and Industry
College of Agriculture

KANSAS STATE UNIVERSITY
Manhattan, Kansas

2012

Approved by:

Major Professor
D.L. Wetzel

ABSTRACT

Chemical imaging enables displaying the distribution of different substances within a field of view based on their fundamental vibrational frequencies. Mid-IR bands are generally strong and feature direct correlation to chemical structure, while near IR spectra consist of overtones and combinations of mid-IR bands. Recently, mid-IR microspectroscopy has enabled determination of the relative substitution of hydroxyl groups with the modifying agent for individual waxy maize starch granules by using synchrotron source. The brightness and non-divergence of the synchrotron source and confocal masking enabled obtaining individual spectra with 5 μm^2 masking and 1 µm raster scanned steps. Each 1 µm step results from the coaddition of hundreds of scans and lengthy data collection is required to produce data. The recent breakthrough at the Synchrotron Research Center uses a multi-beam synchrotron source combined with a focal plane array microspectrometer. This major improvement in localized detection of the modifying agent within single waxy maize starch granules is the increased efficiency of focal plane array detection and an effective spatial resolution of 0.54 µm. Mixtures of granular solids represent an analytical challenge due to the range of heterogeneity and homogeneity within samples. Near IR imaging provides deeper sample penetration allowing for solid mixture analysis. However, the broad, overlapping bands present in the near IR necessitates statistical data treatment. This requires imaging specimens representative of the individual components to create spectral libraries for classification of each component. Partial least squares analysis then allows characterization and subsequent pixel analysis provides quantitative results. The primary break system for wheat milling was studied as it is key in releasing endosperm to be further ground into fine flour in subsequent processes. The mass balance of endosperm throughout individual unit processes was determined by obtaining flow rates of incoming and outgoing millstreams and

calculating endosperm content through pixel identification. The feed milling industry requires the use of a tracer to determine adequate mixing and mix uniformity to limit the time and energy in processing. Near IR imaging allows individual components of a formula feed to serve as a self-tracer, eliminating the need of an inorganic tracer.

TABLE OF CONTENTS

List of Figures

List of Tables

List of Abbreviations

1BK – First break

1M – First midds reduction

2BK – Second break

3BK – Third break

FOV – Field of view

FPA – Focal plane array

FT-IR – Fourier transform infrared

IMS – Infrared microspectroscopy

IRENI – Infrared Environmental Imaging

NA – Numerical aperture

MCT – Mercury-cadmium-telluride

OS – Octenylsuccinyl

OSA – Octenyl succinic anhydride

PLS – Partial least squares

RMS – Root mean square

SIZ – Sizings

SNR – Signal-to-noise ratio

SRC – Synchrotron Research Center

Acknowledgements

It would not have been possible to write this Master's thesis without the help and support of the people around me, to only some of whom it is possible to give particular mention:

My parents, Larry and Deana Boatwright for their patience and support and giving me constant advice, whether I wanted to listen or not.

The Department of Grain Science and Industry for supporting me and giving me a chance to continue my academic career.

My undergraduate advisor, Kendall McFall, who gave me my first step in the right direction.

My former labmates Hicran Koc, Emily Bonwell, and Lauren Brewer for showing me the ropes.

My current labmate Tyler Nickoley for being my go to for any assistance.

My committee members, Dr. Jeff Gwirtz, Dr. Paul Seib, and Dr. Yong Cheng Shi for their insightful comments and tough questions.

My advisor, Dr. David Wetzel for his continuous support towards my MS study and research and his patience, motivation, enthusiasm, and immense knowledge.

Part 1: Introduction

1.0 Mid-IR Spectroscopic Imaging

Mid-IR microspectroscopic imaging has developed into a widely used technique in the study of the molecular chemistry of many different materials. The combination of infrared spectroscopy with light microscopy has enabled locating specific areas of samples on a microscopic level and obtaining molecular information (1, 2). The first use of a microscope as an attachment to a mid-IR spectrometer was introduced in 1950's (3). The practicality of microspectroscopic measurements was later improved by the combination of Fourier transform infrared (FT-IR) spectrometry and highly sensitive detectors (4). Messerschmidt and Sting patented the first research FT-IR microscope in 1989, featuring a globar source and a liquid nitrogen cooled mercury-cadmium-telluride (MCT) detector. The Spectra Tech IR-PLAN^{TM} used a Schwarzschild front surface objective and a condenser with confocal remote image plane masking. The confocal masking resulted in increased spatial resolution and spectra more representative of the target region sampled.

The mapping capability of infrared microscopy was subsequently enhanced in 1990 with the introduction of the Spectra Tech IRμs^{TM} with a microprocessor controlled stage and a decrease in the optical path, which improved signal throughput. Another significant advancement to infrared microspectroscopy was the utilization of a synchrotron source. The first synchrotron infrared microspectroscopy experiment was performed on beamline U2b at the National Synchrotron Light Source (NSLS) in 1993 (5). A synchrotron source provides brightness 100-1000 times greater than the traditional globar source, resulting in increased spatial resolution and a higher signal to noise ratio (SNR). This advance resulted in the ability to image single cells and parts of cells (6-8).

In 1994, the focal plane array (FPA) detector was introduced as an alternative to the single element detector (9, 10). An array of individual detector elements allowed simultaneous collection of spectral data for multiple pixels, measuring the frequency with an interferometer. Subsequent advances were made to increase the spatial resolution of SNR for FPA infrared microspectroscopy, but the quality of FPA spectral data with a globar source remained inferior to confocal operation. Carr et al. (11) proposed an enhancement to FPA microspectroscopy with the potential of a synchrotron source (Figure 1.1). Multiple uses of synchrotron sources with FPA detection (12, 13) were designed by pioneering groups using single synchrotron beams. In 2010,

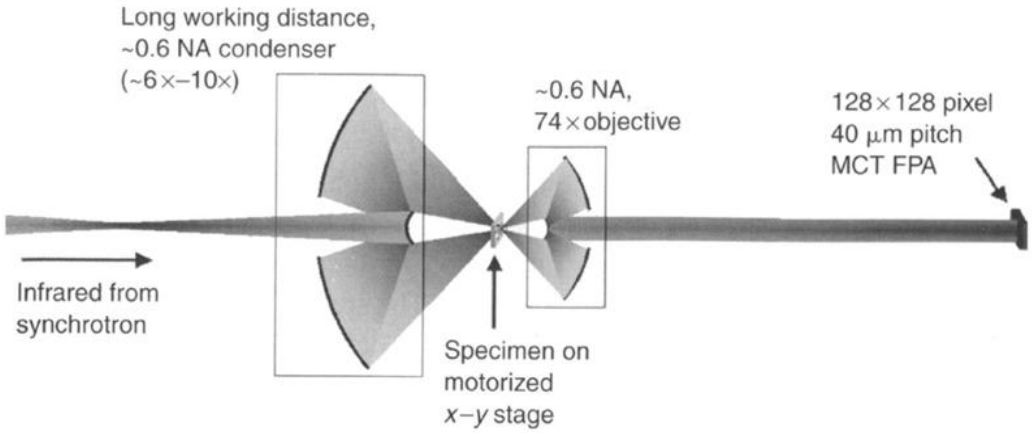

Figure 1.1 Diagram of the optical configurations with high numerical aperture (NA) objective necessary for use of a microspectrometer with mercury-cadmium-telluride (MCT) focal plane array (FPA) detection utilizing a bright synchrotron source. [Reprinted from 11]

a University of Wisconsin-Milwaukee research group at the Synchrotron Research Center (SRC) designed a multi-beam synchrotron FPA microspectrometer system called the Infrared Environmental Imaging (IRENI) beamline, which provided increased spectral resolution (14).

1.1 Near IR Spectroscopic Imaging

While the first combination of a microscope and mid-IR spectrometer was achieved in the 1950's, pioneering work in near IR transmission spectroscopy was being performed by Kaye of Beckman Instruments (15, 16). Later, diffuse-reflectance measurements in the near IR were used for routine quantitative analysis in the agriculture commodity industry using multivariate statistical analysis at multiple wavelengths. Diffuse reflectance occurs when lights enters a sample and is scattered within the sample matrix. The scattered light may then pass through multiple scattering-absorption events before reflecting back toward the optics and detector elements (Figure 1.2). Mid-IR diffuse reflectance measurements typically require application of

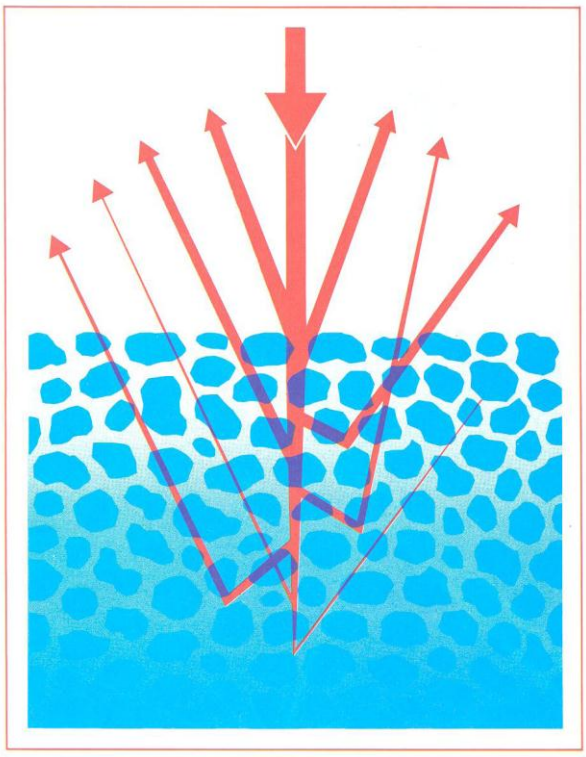

Figure 1.2 Visual representation of diffuse reflectance pathways through a granular sample. [Reprinted from 17]

the Kubelka-Monk function for spectral correction, but this is not required for quantitative near IR analysis due to weaker absorption bands.

Near IR spectroscopic imaging was first performed in 1990 using a CCD video camera and narrow band interference filters (18). Due to a need in the pharmaceutical industry, a tunable-filter near IR imaging spectrometer with FPA detection was developed by Spectral Dimensions, Inc. The use of a liquid crystal tunable filter (LCTF) allowed electronic wavelength switching. Near IR imaging with an FPA allowed detector enabled nondestructive, rapid measurements of a sizable field of view (FOV). This technology has enabled the detection of germination of wheat kernels (19), bacterial identification (20), mass balance of wheat milling intermediates (21), and various pharmaceutical applications (22, 23).

Part 2: Multi-Beam Synchrotron Microspectroscopic Analysis of Individual Chemically Modified Starch Granules

2.0 Introduction

The major product of the uptake of carbon dioxide via photosynthesis is carbohydrate polymers. The majority of the carbohydrate is used for starch-hydrolysis (refinery) products, while the remaining native starch is used for various polymeric products, about 20% of which are used in the food industry as food ingredients (24). In higher plants, starch is universally biosynthesized as granules (representing the basic unit of starch). For cereal grains, the starch granules vary in size from 2 to 30 um in diameter, with waxy maize starch granules typically ranging from 5 to 20 um (25).

Chemically modification of starch is used in industry to improve upon the properties of native starch. One such modification greatly improves the emulsifying and encapsulating properties of starch for use in various products. This modification is achieved by esterifying starch granules by reaction with a measured quantity up to 3% based on starch of oct-2-enyl succinic anhydride (OSA). The hydrophobic nature of the octenylsuccinyl (OS) hydrocarbon chain together with the hydrophilic OH groups on starch generates an amphiphilic polymer, which is especially useful for emulsification and encapsulation. A common use of an OS starch is to emulsify the hydrophobic oil of orange used to flavor orange sodas. Because chemically modified starches are manufactured in very large batches, maintaining uniformity within batches is of concern. Ideally, each individual starch granule would be esterified, and the percentage of the ester substitution on each granule would be uniform within and between each batch.

The spectral features of carbohydrates are well known from dispersive mid-IR spectroscopy (27, 28) in a transmission mode applied to samples in a Nujol mull or a KBr pellet. FT-IR spectroscopy on a macro scale, applied to starch, has been reported by multiple research groups (29-32). Analysis of individual starch granules is, therefore, a reasonable experiment to perform. The spatial resolution of FT-IR microspectroscopy enables the microstructure to be revealed at the level of individual starch granules.

The emulsifying function of OSA modified starch occurs on a small scale at multiple hydrophobic sites on the surface of each granule; therefore, its effectiveness is dependent on intragranular as well as intergranular uniformity. Intergranular evidence of the chemical modification was reported by Bai et al. (33) by taking a census of ester carbonyl for more than 350 individual starch granules, via FT-IR microspectroscopy obtained from a 15 μm ×15 μm area within flattened granules in a reflection absorption mode. The carbonyl band at 1723 cm^{-1} band was compared with the complex carbohydrate band centered at 1025 cm^{-1} to reveal the presence of the ester carbonyl. Intragranular distribution of the ester population required FT-IR microspectroscopy with a synchrotron source (34). The carbonyl 1723 cm^{-1} band area was compared with the 1143 cm^{-1} band representative of the complex starch band centered at 1025 cm^{-1} to reveal the localized presence of ester.

The first intragranular study of modification within waxy maize starch was performed at NSLS in 2010 using a confocal Continμum™ IMS (Spectra Tech/ Nicolet, Shelton, CT), with a single liquid nitrogen cooled MCT detector and 1 μm steps in a raster scan mapping procedure with a 5 μm x 5 μm image plane masking (34). The current state-of-the-art experiment was performed using the multi-beam synchrotron source and FPA spectrometer at the SRC. The OSA modified starch studied at SRC were prepared at the same time as the 2010 article**.** The two

synchrotron experiments are compared in order to show the experimental leap with the multi-beam synchrotron source with FPA detection.

2.1 Experimental

2.1.1 Instrumentation

The experiments on single modified waxy maize starch granules were performed on the unique IRENI beamline at the Synchrotron Research Center, University of Wisconsin-Milwaukee, Stoughton, WI. The theoretical potential image fidelity enhancement utilized at the SRC was first proposed by Carr et al. (11), recommending the use of a high magnification Schwarzschild objective from the synchrotron illuminated field of view on the microscope stage to a cooled commercially available FPA. The microscope and detector optical scheme was subsequently implemented at the SRC using a multi-beam synchrotron source combined with a FPA microspectrometer in the optical configuration, shown in Figure 2.1 (35). The IRENI

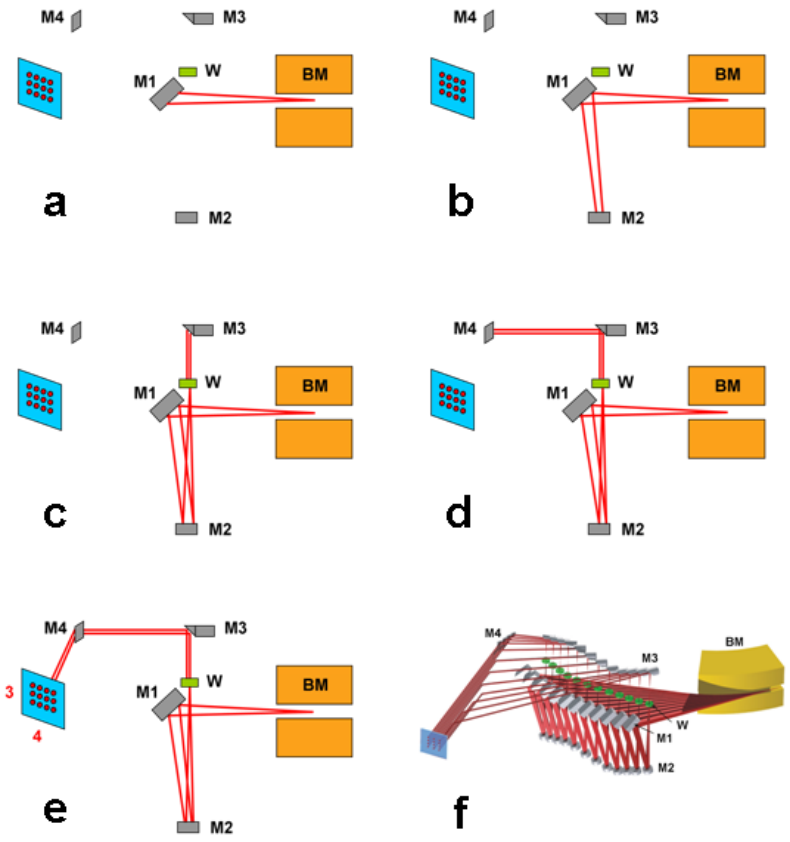

Figure 2.1 Five step diagram of a single synchrotron beam reflection pathway in a high vacuum, from the bending magnet to a plane mirror (a), then to a parabolic mirror (b) to move the beam out of the axis of the storage ring. The beam emerging from the ZnSe window (c) enters a nitrogen purged chamber where a third (d) and fourth mirror (e) direct the beam to the microscopic target. Eleven other beams are treated similarly to produce a recombined 4 × 3 matrix (f) that constitutes the combined multi-beam synchrotron source. [Reprinted from 35]

beamline extracts a 320 mrad horizontal × 25 mrad vertical swath of radiation from a single, dedicated bending magnet. The radiation is first separated by a set of 12 toroidal mirrors in a vacuum chamber. A set of 12 flat mirrors then guide the beams out of the vacuum chamber through zinc selenide windows. The beams are then collimated by 12 parabolic mirrors before they are rearranged into a 3 x 4 matrix by 12 stacked flat mirrors. An optical feedback system follows to stabilize the beam swath, increasing the SNR. The beam swath is then sent to a Bruker Vertex 70 spectrometer (Billerica, MA) coupled to a Bruker Hyperion 3000 infrared microscope. The beam swath then passes through a 20x Schwarzschild condenser (NA=0.6) before

illuminating the sample on the stage. The condenser focuses the beam at a deliberate slight defocus to allow overlap of the individual beams to obtain fairly homogeneous illumination. The sample is then imaged through a 74x objective (NA=0.65) onto a 128 pixel x 128 pixel FPA. Utilizing the inner 64 pixels x 64 pixels of the FPA resulted in an effective 0.54 um x 0.54 um pixel dimension.

In each case, data were obtained from the center of the flattened starch granule. A transmission mode was used for the IRENI imaging with a flattened granule mounted on a barium fluoride 13 mm diameter, 1 mm thick window. To compare individual starch granule data, spectra from an approximately 10 μm × 10 μm area in the center of each granule were treated to produce an image that described the carbonyl chemical topography of the flattened starch granule. All IRENI images were acquired with Bruker OPUS© software, with the spectral resolution of 8 cm^{-1} and 256 coadded scans being sufficient for an acceptable SNR.

2.1.2 Sample preparation

The modified starch granules studied were the product of reacting commercially available waxy maize starch granules (Corn Products Inc., Bridgewater, NJ) in a slurry with 9.0% (starch basis) octenyl succinic anhydride under carefully controlled conditions (pH 8.0 and 25 °C) by Bai et al., as described elsewhere (33). The esterified specimen with an OS degree of substitution of 0.056 was rinsed with successive portions of distilled water until no acidity from the reagent was detected and then dried. Under a low powered microscope, the starch granules were flattened with a small 7 mm diameter stainless steel roller on the surface of a 1 mm thick BaF_2 window. This was necessary to obtain a thickness that would allow transmission of infrared light.

2.1.3 Data Processing and Analysis

The IRENI imaging data were subsequently processed with OPUS© software (Bruker, Billerica, MA). A baseline corrected band area ratio map was produced for each image to show the relative concentration of ester carbonyl (1723 cm-1). The ester carbonyl band area was ratioed to the area of a representative carbohydrate band (1148 cm-1), which served as an internal standard to allow correction for any differences in thickness across the area sampled (Figure 2.2). The range used for the ester carbonyl band area was 1764 cm-1 to 1687 cm-1, while the range used for the calculation of the representative carbohydrate band area was 1183 cm-1 to 1121 cm-1 with a baseline from 1181 cm-1 to 1066 cm-1. A false color scale was used to show the relative concentration of ester carbonyl from low to high, with red and yellow respectively.

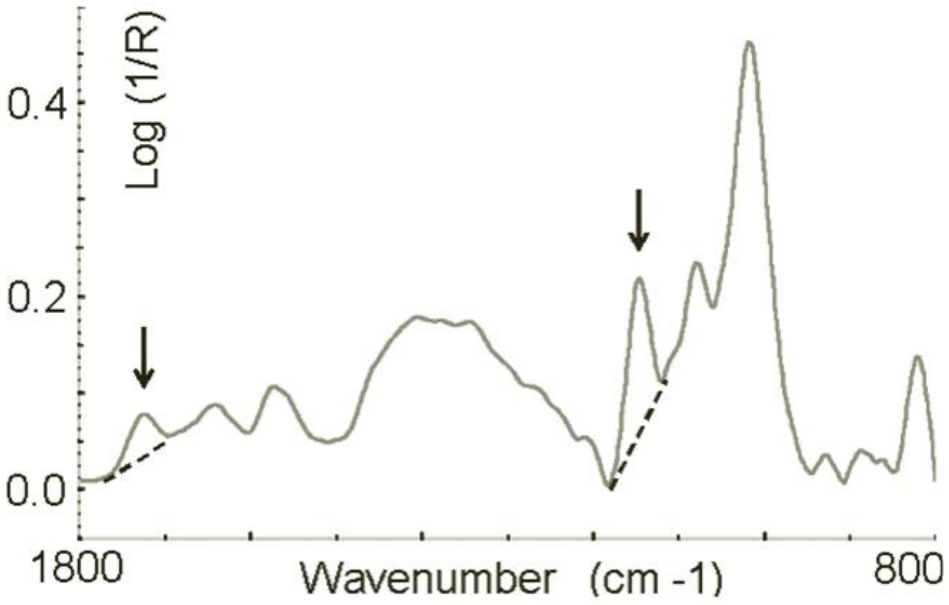

Figure 2.2 The typical fingerprint region spectrum of an OSA modified (9%) waxy maize starch granule illustrating the baseline corrected absorbance bands for carbonyl (1723 cm-1) and starch (1148 cm-1). [Reprinted from 34]

2.2 Results and Discussion

Modified starch imaging results from the IRENI were compared with those obtained from a previous short step confocally masked synchrotron IMS experiment to highlight the instrumental advance. The baseline corrected band area ratio results were dependent on the numerical values obtained from the spectra of each pixel. For these synchrotron IMS experiments, the image fidelity registers the difference on the z-axis between pixels that are adjacent on the x,y plane. Two important criteria examined for comparison were the absorbance range detected and the ability to distinguish between the peak area ratios of adjacent pixels in the image. With a figure of merit for comparison defined as the ratio of maximum z-axis value to the threshold value, both criteria are accommodated. Comparing the multi-beam synchrotron FPA ratios (0.52:0.07 = 7.4) to the short-step confocal ratios (0.66:0.32 = 2.0), results in a 3.6 times improvement on the former. Thus, the sensitivity to 3D topographic differences of functional group absorbance values shows significant improvement. Furthermore, the contrast between adjacent pixels shows the effect of IRENI optics in achieving the theoretical point spread function (PSF) for a Schwarzschild optic as shown in a recent *Nature Methods* article (35). In **Figure 2.3**, the baseline corrected peak area ratios of the carbonyl band at 1723 cm^{-1} to that of a representative carbohydrate band centered at 1148 cm^{-1} are plotted by their x,y coordinates. Beyond the threshold established by the granule minima, the ratio varies greatly between adjacent pixels in numerous cases. This observable variation is a result of the

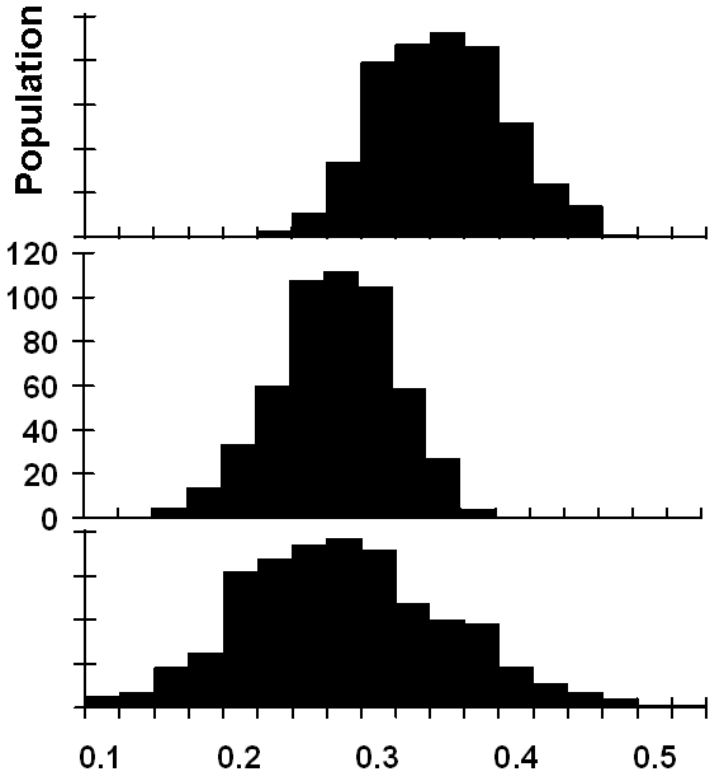

Figure 2.3 Histograms of the population of the intragranular peak area ratio of carbonyl/starch (1723 cm^{-1}/1148 cm^{-1}) for each pixel within each of three individual modified starch granules.

combination of the 74× objective and the 64 × 64 element FPA with 0.54 μm increments. From the IRENI data, the root mean square (RMS) noise level was 6 mA units, determined from the range of 2100 cm^{-1} to 1900 cm^{-1} where no absorption occurred. This is in contrast to an RMS noise level of 8 mA measured for the light limited confocally masked beam used in the previous experiment.

The baseline corrected band area ratio maps (Figure 2.4) of two of the granules (1 and 2) show a large number of peaks and valleys within the approximately 11 μm × 11 μm selected area. Note that across the x, y plane, numerous z-axis excursions are seen among neighboring pixels. The numerical values obtained allow comparison between the individual granules

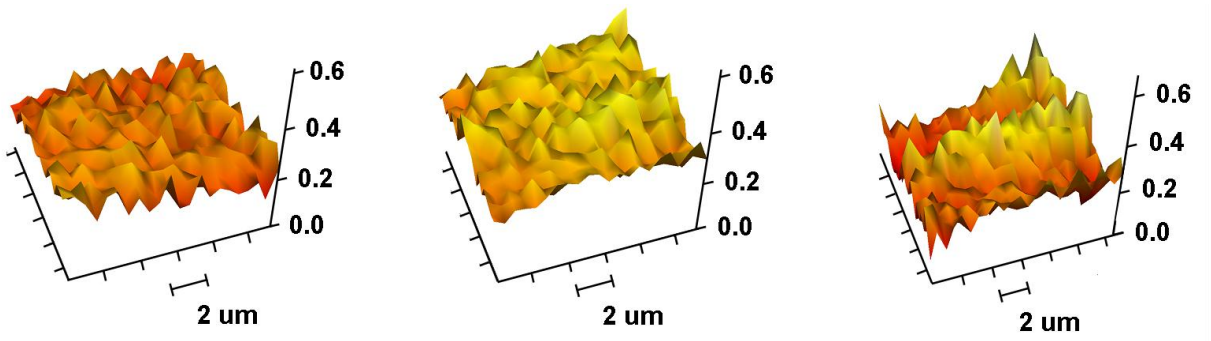

Figure 2.4 Chemical images based on the peak area ratio of ester carbonyl (1723 cm-1) to the representative starch band (1148 cm-1), taken from the center of three flattened modified starch granules. Pixels with high carbonyl content are highlighted by a yellow false color. Note the greater excursion in the third image; revealing a physical defect in the granule.

represented in the figure. The difference between the individual granule peak area ratio from the average value and the threshold value for each pixel differed from 0.2 to 0.25 to 0.45 between the three granules. The ranges from low to high were also revealed. These intergranular observations are summarized by histograms shown in Figure 2.5. Examination of the data for the three granules in all three forms (3D image, bar graph, and histogram) revealed a significant

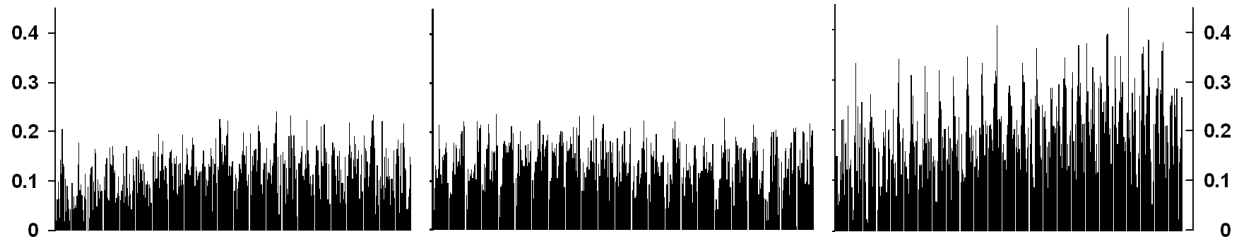

Figure 2.5 Bar graphs illustrating the difference in the peak area ratio of carbonyl/starch (1723 cm-1/1148 cm-1) for each individual image pixel in sequence. The calculated ratios exceeding the carbonyl detected threshold of the image are plotted for each of the three granules shown.

localized aberration for granule 3. Examination of the photomicrograph for granule 3 (Figure 2.6) showed a physical depression within the FOV. This observation explained the chemical

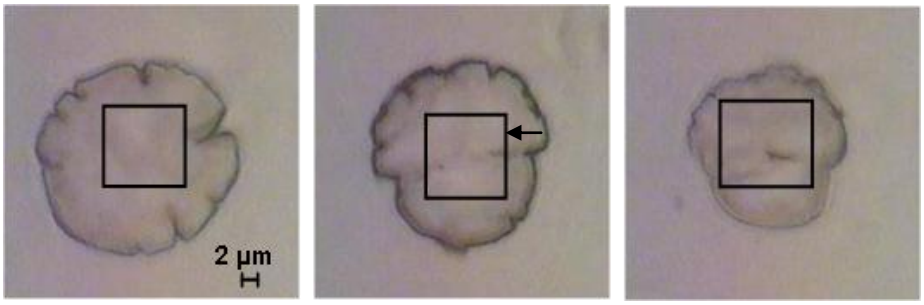

Figure 2.6 Photomicrographs of the granules imaged in Figures 2.3, 2.4, and 2.5, with a box designating the area from which spectra were extracted for analysis. Note the physical deformation in the photomicrograph of granule 3, corresponding to the high variation shown in the third image of Figure 2.4.

topographical inconsistency found from treating the spectroscopic data obtained in the image.

2.3 Summary

Prior to introduction of the IRENI multi-beam synchrotron FPA dedicated system, confocal synchrotron imaging was shown to be far superior to that of a conventional FPA instrument. The IRENI beamline, on the other hand, not only offers the high speed of parallel data acquisition of the FPA, specifically designed to allow real time experimentation with living organisms. As previously reported by others (35), the enhanced image fidelity that appears in the 3D mapping of IRENI data results from an expanded z-axis contrast and improved spatial definition on the x,y axes. Greater difference between the optical expanded scale response of adjacent pixels is achieved because of the extreme brightness of the multi-beam synchrotron source well exceeding any source noise. The differing values between individual pixels on the x,y axes is the experimental performance result of approaching the theoretical point spread function of 1.0λ with the Schwarzschild optic discussed by Carr (11, 36) as opposed to 1.22λ with a conventional lens.

Part 3: Break System Analysis of Flour Milling Intermediate Solid Mixtures via Near Infrared Focal Plane Array Chemical Imaging

3.0 Introduction

The wheat milling industry, having multiple intermediate processing streams and individual unit processes, provides many opportunities for chemical analysis. Milling is a low-margin process, thus a single change can have significant consequences. Thus, various processes in the milling process need to be optimized in order to obtain the maximum endosperm yield. The key product in the milling industry is flour (endosperm). Endosperm is typically 83% of the composition of a kernel of wheat (37). Additional byproducts of flour milling can include clean bran and germ. Typical straight grade flour extraction ranges from 72-75% (38). Ultimately, the efficiency of a flour mill is determined by the ability to maximize flour extraction while avoiding contamination with bran and germ.

Analyzing the endosperm purity of milling fractions has always been a difficult problem because we are dealing primarily with a mixture of organic solids. The standard measure is ash determination, which measures the inorganic residue remaining after combustion of an intermediate stream. Wheat milling fractions contain several materials besides endosperm; lumping these residual organic components together as non-endosperm simplifies analyses as binary mixtures. Among the non-endosperm components are the germ, aleurone cells, aleurone cell walls, and pericarp. An analytical chemical procedure for milling fraction analysis using the technique of spectroscopic imaging was developed at Kansas State University (21). This spectroscopic method targeted mixtures containing varying amounts of wheat endosperm and non-endosperm. In each case, parts of the fraction are considered product and all others are

considered byproducts that may be subject to rework. For each individual material that comes from a "unit process" such as a roll stand, purifier, or sifter, the calculated purity quoted as endosperm (product) concentration multiplied by the quantity (expressed as weight or flow rate) produces the endosperm yield for a particular intermediate stream. Subsequent analysis of intermediate streams leaving a unit process enables endosperm mass balance calculation and direct, objective assessment can be made.

In the first application of this method (21), Figures 3.1 and 3.2 show the endosperm yield of the inbound stream and outbound intermediate product and byproduct streams of a single purifier (21). The imaging results on these purifier specimen sets were produced in the Microbeam Molecular Spectroscopy Laboratory and the intermediate streams specimen sets were from a commercial mill. The two sets of specimens were produced to show maximum contrast. Figure 3.1 shows specimens taken before adjustment of purifier variables, which resulted in a higher yield of purified endosperm; whereas Figure 3.2 was after adjustment. Previews of applying the quantitative near IR imaging direct endosperm determination method to specific teaching situations have been reported by Gwirtz (39, 40). In the latter case, the Ross Walking mill was operated to simulate a double high first and second break (1BK/2BK) configuration followed by sieving with nine progressively smaller sieves (1041-132 µm).

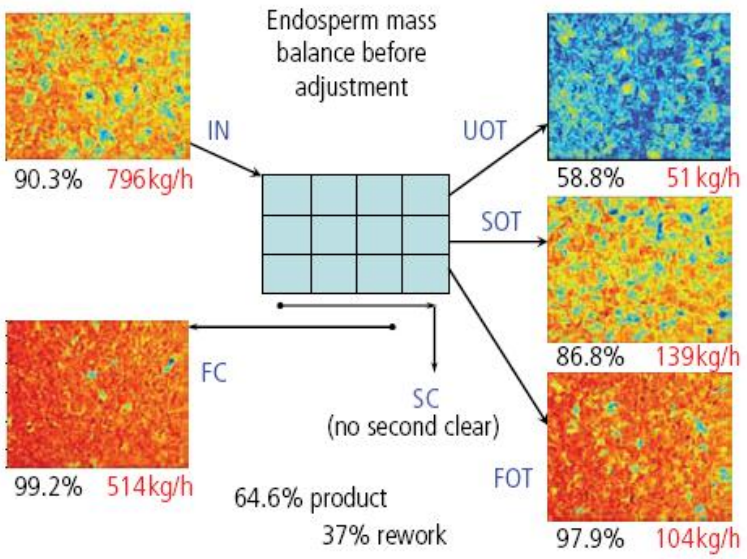

Figure 3.1 Endosperm mass balance of a commercial flour mill purifier before adjustment. The endosperm mass flow rate (kg/h) of each stream was calculated from the NIR endosperm content and the mass flow rates (not shown) of the streams. From the input (IN) to the first (FC), endosperm content was enriched from 90.3% to 99.2%, whereas the quantity was reduced from 796 kg/h to 514 kg/h. The byproduct material was divided into three streams designated as upper overtails (UOT), second overtails (SOT), and first overtails (FOT) of varying percentage endosperm and endosperm flow. Before adjustment, a 64.6% product yield resulted in 37% byproduct subject to rework. A false color scale is used to highlight endosperm and non-endosperm with warm (red) and cool (blue) color, respectively. [Reprinted from 21]

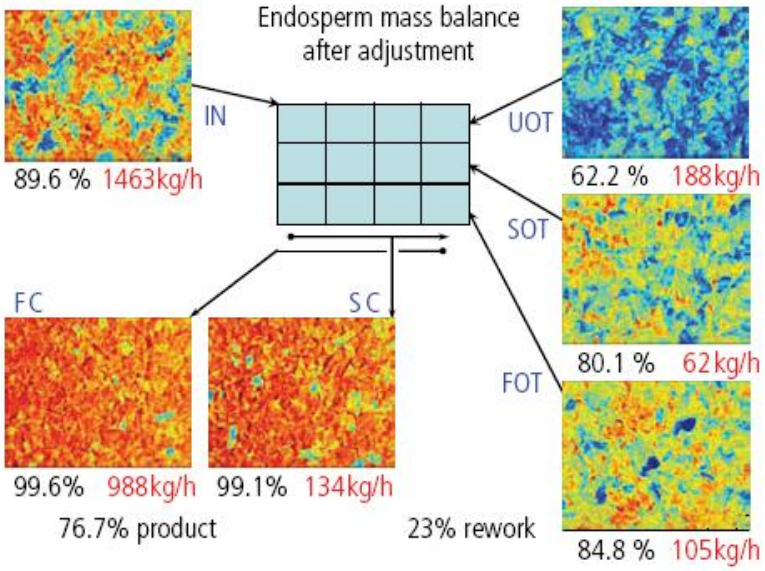

Figure 3.2 Endosperm mass balance of a commercial flour mill purifier after adjustment. In contrast to Fig. 3.1, the summation of the FC and SC product was 76.7%, and the combined byproduct streams subject to rework was 23.3%. [Reprinted from 21]

.Millers typically optimize the break release for every grinding operation within a mill, with special attention to the primary breaks, which affect intermediate stock distribution, quantity, and quality. This has been emphasized by the introduction of programmable roll adjustment of break releases (41) and pre-set break roll gaps that automatically change settings upon changing wheat mix to a mill (42). Millers have traditionally used trial and error to achieve optimization. Our study conducted here, utilizes a quantitative near IR imaging method developed at Kansas State University to assess the results of variation of 1BK/2BK roll gap. This procedure enabled endosperm analysis of intermediate products derived from the primary break unit processes (1BK, 2BK, 3BK) in flour milling. Using the quantitative near IR imaging technique for this purpose, we assume a binary mixture of endosperm and non-endosperm.

For quantitative near IR imaging spectral libraries of the individual components must be acquired as standards, by subjecting pure forms to chemical imaging to produce a multivariate spectroscopic characterization. Characterization of each standard material was determined using multiple wavelengths to produce a recognizable signature for each one. This allowed identification of each of the 82,000 pixels in the images of experimental streams obtained from the mill. Quantitation is subsequently achieved by a mathematic algorithm using the endosperm and non-endosperm characterization images. This method was then used to quantitate the endosperm leaving the primary break system for several 1BK/2BK roll gap settings and to objectively compare intermediate streams between an optimal and suboptimal primary break operation.

3.1 Experimental

3.1.1 Instrumentation

A Sapphire™ model indium antimonide (InSb) focal plane array (Malvern Instruments, Columbia, MD) imaging system was used. A simplified diagram of the instrument used is shown in **Figure 3.3**, where light emitted from four quartz tungsten halogen illuminating lamps is

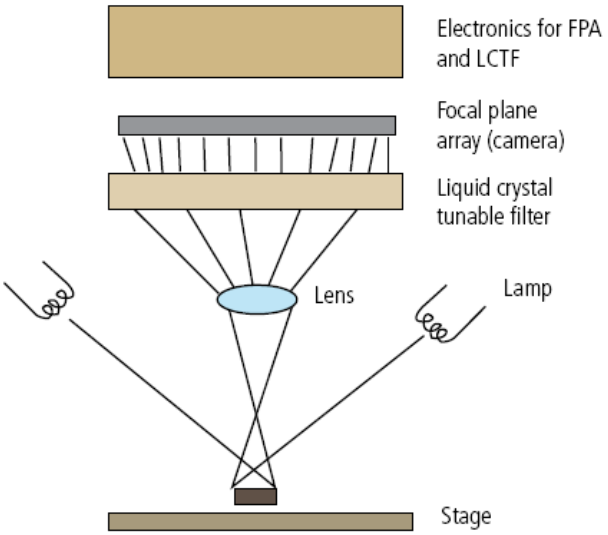

Figure 3.3 Optical diagram of the near IR FPA imaging system. [Reprinted from 39]

reflected diffusely off of the sample on the stage and captured by a lens in the instrument. From the lens, the light passes through the liquid crystal tunable filter (LCTF), which sorts out the wavelengths in sequence. The selected wavelength range for this instrument, 1200-2400 nanometers, goes to FPA of InSb sensors that produces an 320 x 256 pixel image. Each pixel within the image FOV is from the response of an individual InSb sensing element of the FPA. As the filter sequentially changes the wavelength, a complete spectrum is produced in each of approximately 82,000 locations in the sample FOV. Before analysis, the instrument is turned on and the SapphireGo data acquisition program was used to initialize the instrument. After initialization, a dark data cube is obtained by scanning a metal mirror for high specular

reflectance and a background data cube is obtained from a white ceramic plate with high diffuse reflectance.

The granular sample material is placed in a stainless steel planchette and covered with a 1-in. × 1.5-in. glass microscope slide. After the material is flattened under the glass and placed on the sample stage, the spectra were taken with a LCTF spectrometer (no moving parts) that provided electronic wavelength switching prior to the parallel waves striking the thermoelectrically (TE) cooled InSb FPA. The only radiation collected by the lens of the imaging system, also defines the FOV, was from the near-infrared source, striking the diffusely reflective specimen at a 45-degree angle. The image intensity of each pixel was mathematically converted to Absorbance, which describes optical density. This step is used to produce a numerical value that is linear in terms of the concentration of the mixture component targeted, and this was done at each optical frequency for each pixel. In the data produced for this report, the imaging lens produced a 13 mm x 10 mm FOV that resulted in a 40 μm calculated pixel size. To provide reliable detector response, the near IR camera is programmed to coadd measurements for a period of 4 minutes. When coarse granular heterogeneous specimens are analyzed, three FOVs were averaged to avoid localized sample differences.

3.1.2 Specimens and Procedure

For each type of wheat used in the mill, the miller must set the break release, which is the main way that a miller can optimize the efficiency of the system via material distribution. Accurate break release adjustment combined with optimal tempering will guarantee good flour extraction and quality. The release from the primary breaks in the mill affects the distribution of all intermediate stocks in the system (38). A two-part study was conducted with the Ross

walking mill laboratory setup utilizing three first break (1BK) settings and three second break (2BK) settings with a fixed setting for third break (3BK), Sizings (Siz), and first Midds (1M) reduction in a single replication to determine if near IR focal plane array quantitative imaging could detect differences in endosperm released from the primary breaks. The 1BK gap settings were 0.020, 0.022 and .024 in. (0.508, 0.559, 0.610 mm), and the 2BK gap settings employed were 0.010, 0.012 and 0.014 in. (0.254, 0.305, 0.356 mm). 3BK was set at 0.003 in. (0.076 mm), Siz gap was 0.005 in. (0.127 mm), and 1M (reduction) was 0.001 in. (0.025 mm). The diagram in Figure 3.4 shows the sieve layout. Three different roll gap settings for 1BK and 2BK resulted in nine different 1BK/2BK combinations for the first group of experimental millings.

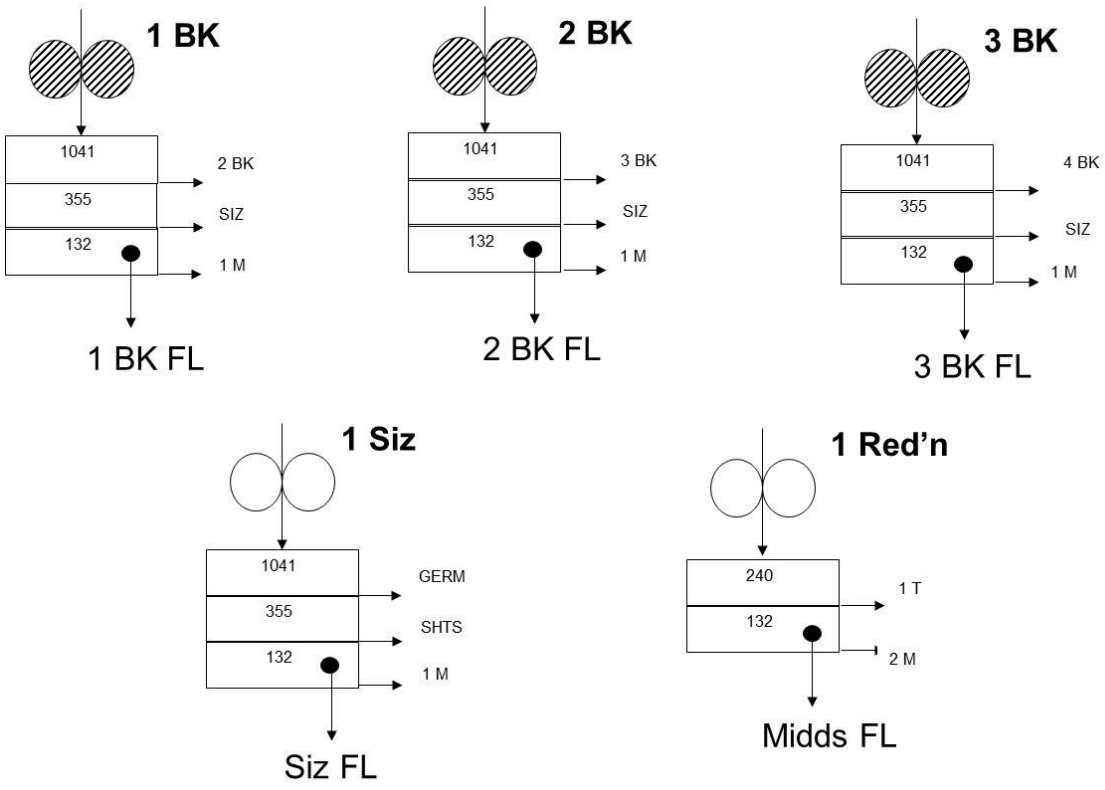

Figure 3.4 Sieve box configuration and stock destinations for a 1BK, 2BK, 3BK, Siz, and 1M milling operation.

The primary milling experiment to optimize endosperm yield was carried out on the same day with 1000 g from the same lot of tempered hard red winter wheat. This experiment focused on the use of quantitative near IR imaging to determine the percentage endosperm content in the physically combined flour, sizings, and reduction streams, respectively, from 1BK, 2BK, and 3BK. From the nine millings in which different 1BK and 2BK gap combinations were used, it was necessary to deliver the intermediate products of the breaks to the successive process to ensure accurate weights of each material. We conducted a second milling experiment later using a stop-flow method to show a snapshot of intermediate byproduct fractions for each unit process for two different gap settings. The subsequent milling on a later date of 1500 g of wheat with two 1BK/2BK combinations was focused on the quantitative near IR imaging of the intermediate products. In this case, 40 g of each intermediate was retained to enable imaging of three replicates of each.

Spectra were collected in triplicate for each sample (single samples were collected for flours) in the range of 1200–2400 nm and processed using Malvern ISys^{TM} 4.0 chemical imaging software. Spectra were first converted to Absorbance. The wavelength segments 1200–1539 and 1851–1999 nm were then removed to eliminate water bands. The spectra were baseline corrected and normalized. Prior to any quantitation, we acquired spectral libraries based on approximately 164,000 spectra from clean bran that was ground (non-endosperm standard) and purified 1M top stock from the Kansas State Pilot Mill (endosperm standard). Each pixel in the binary mixture was subsequently identified using both the multivariate characterizations of A (endosperm) and B (non-endosperm). We then used an algorithm of the two characterizations [A / (A+B)] to establish the decimal fraction of endosperm in the milling samples. The product of stream

sample weights and their calculated endosperm content enables quantitation of endosperm mass flow.

We use the term "endosperm yield" to indicate the amount of endosperm released from the first three breaks; for each fraction leaving the break system, it was the product of the weight fraction (weight of the fraction divided by the total weight of wheat milled) and the NIR imaging percentage endosperm. $$Endosperm\ yield = \frac{\sum (Fraction\ Weight \times Percentage\ \ Endosperm)}{Total\ Weight\ Wheat\ \ Milled}$$

Using this calculation for each break flour, break to sizing fraction, and the break to reduction fraction, we obtain the endosperm yield.

3.2 Results and Discussion

An AOM Technical Committee Survey by Wingfield (43) related to break release and flour extraction indicated that the overall extraction percentage of flour and/or semolina that a mill can obtain is established in the break system, where the endosperm is removed from the bran coat. Further importance is place on the primary break system, as Li and Posner (44) showed that setting the break release of 1BK and 2BK significantly affects sizings stock and total flour production. Results of the various break gap settings visually show the differences in endosperm separation based on the presence of contamination from non-endosperm parts of the kernel. Quantitative analysis of the milling process, shown in Figure 3.4, required retaining the majority of intermediate products. The three-dimensional Figure 3.5 shows the endosperm yield values for the nine 1BK/2BK pairs of settings on the z-axis. The high (75%) and low (67%) values. Observations between these two combinations are summarized in Table I.

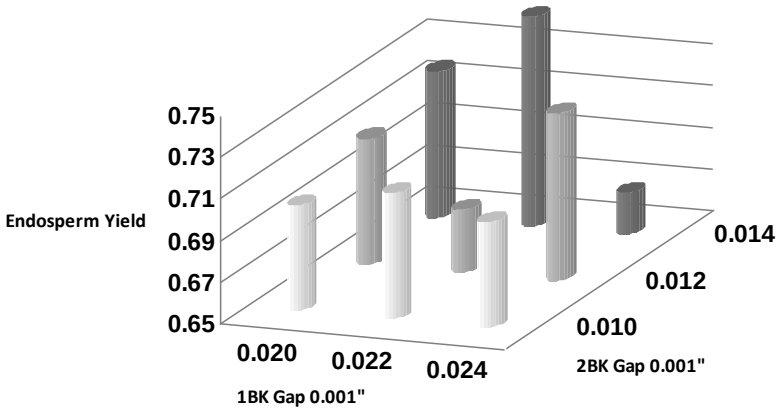

Figure 3.5 The endosperm yield (near IR calculated endosperm released from the primary breaks) is shown for all of the nine 1BK/2BK gap setting combinations.

Table I. Comparison of optimal (.022/.014") and inferior (.024/.014") 1BK/2BK gap settings

	Optimal	Inferior
Endosperm to 4BK (grams)	82	157
Purity of break flour	99%	92%
Purity of cumulative material from break to reduction	100%	95%
Purity of cumulative from break to sizings	90%	79%
Purity of sizings flour	100%	97%
Purity of sizings stock sent to reduction	100%	94%
Purity of reduction stock sent to second reduction	94%	84%

Figure 3.6 reveals the calculation of endosperm yield for the high and low 1BK/2BK gap pair settings by multiplying the quantity of endosperm obtained from the flow rate or weight of the product by the endosperm content as determined from chemical imaging data. Although the masses of the cumulative flour, sizings stock, and reduction stock were relatively unchanged among different roll gap setting, the greater purity of the 0.022/0.014 in. 1BK/2BK gap pair settings accounts for the high endosperm yield. To achieve the best quantitative and qualitative performance from a wheat mix, the greater cumulative yields indicate the better roll gap settings.

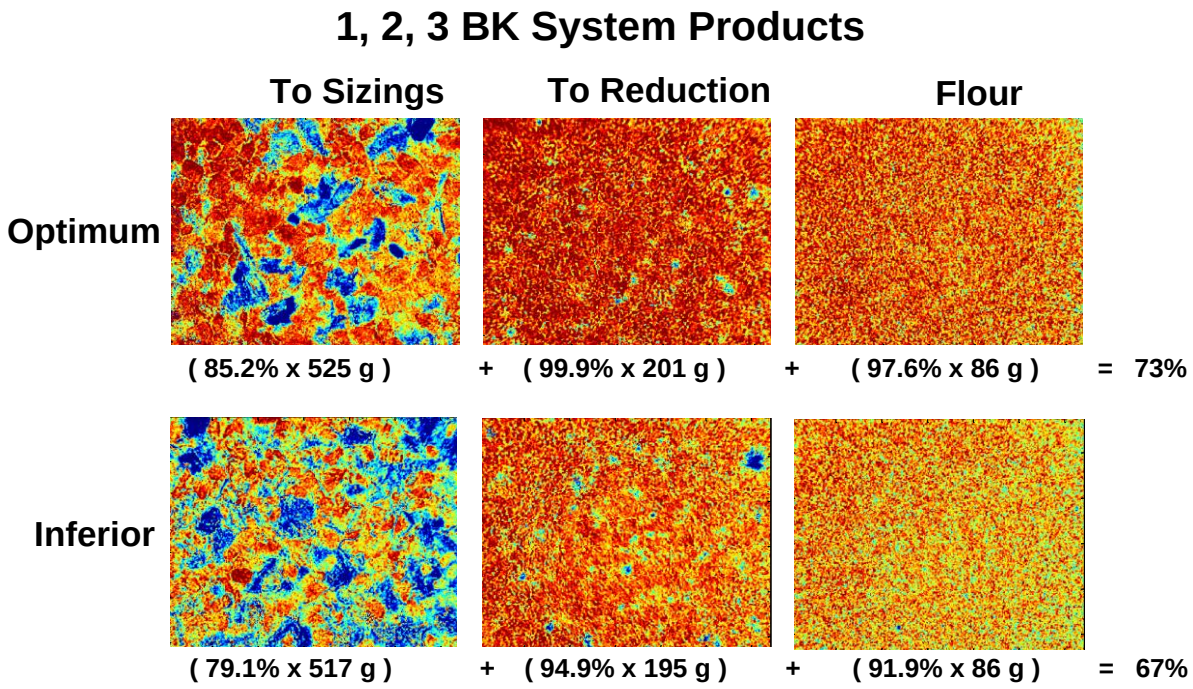

Figure 3.6 Chemical imaging results are displayed for the cumulative break system products (material to sizings, reduction, and flour) for both the optimum and inferior 1BK/2BK roll gap settings. These results are from the milling of 1000 g of wheat. Note the equations that include the endosperm purity and mass of each material, the weight product sums of which equal the endosperm yield. A false color scale is used to highlight endosperm and non-endosperm with warm (red) and cool (blue) color, respectively. Note the higher purity of each of the products and higher endosperm yield of the optimum gap pair milling.

For the secondary milling experiment, we obtained imaging data for all intermediate products of the 1BK, 2BK, 3BK system, as well as a Siz and 1M reduction operation.

Observations from the comparison of corresponding fraction images from the two roll gap settings on their respective calculated purity are summarized in Table II. Figures 3.7-3.9 provide

Table II. 1BK / 2BK Roll Gap Effects

	.022/.010"	.024/.014"
Endosperm to subsequent stages	Greater release of endosperm to subsequent stages	Smaller release from breaks to subsequent stages
Purity of material from 1BK to sizings	80.7%	76.9%
Mass of material from the breaks	Same for both settings	
Endosperm in material to subsequent breaks	Less endosperm	More endosperm
Purity of material from 2BK to sizings	42.1%	77.8%
Flour from sizings	More of Inferior Quality	Less
Purity of reduction material to 1T	89.0%	67.4%

visual evidence of the differences in endosperm purity for intermediate streams from each operation for the two millings. The chemical images in Figures 3.7 and 3.8 both reveal the greater break release for the first milling. Figures 3.8 and 3.9 show that 2BK and 3BK release more endosperm to sizings and reduction, because more endosperm remains on the bran.

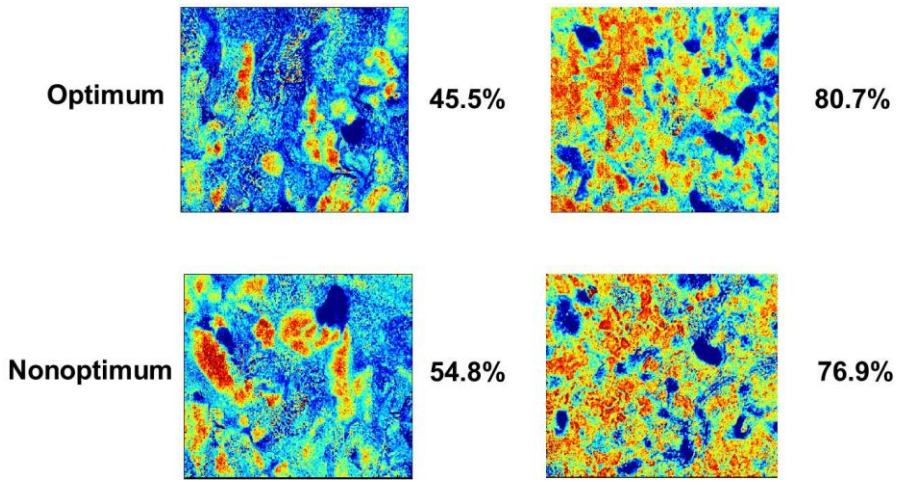

Figure 3.7 Comparison of chemical images and calculated percentage endosperm from 1BK material destined for 2BK (left) and sizings (right) for two millings. Note the additional endosperm remaining in the material to 2BK for the second milling and the endosperm enriched material leaving the first milling to sizings.

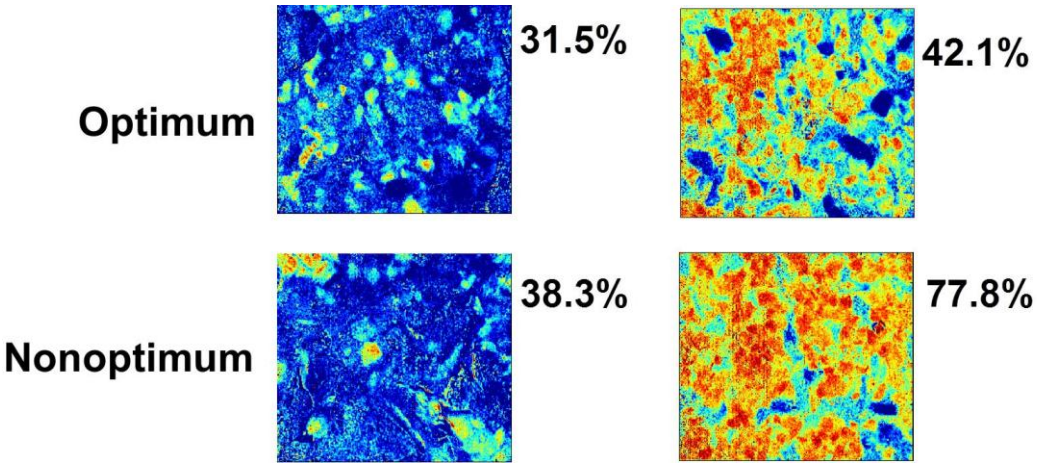

Figure 3.8 Comparison of chemical images and calculated percentage endosperm from 2BK material destined for 3BK (left) and sizings (right) for two millings. Note the additional endosperm remaining in the material to 3BK and heading to sizings for the second milling.

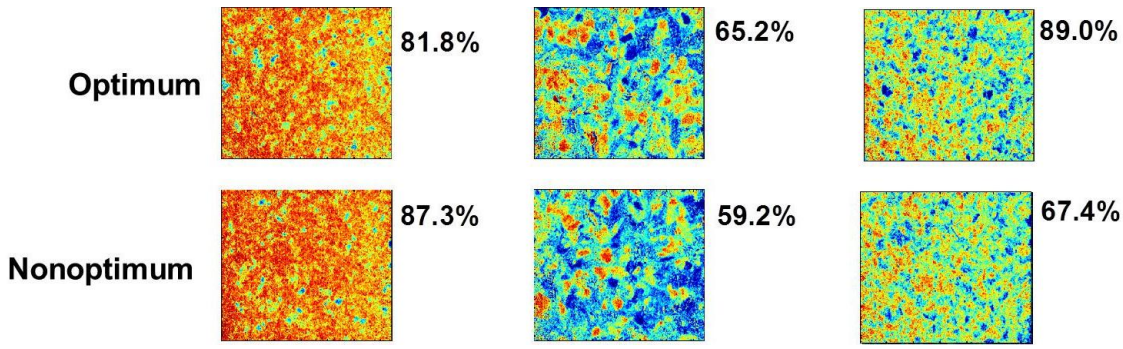

Figure 3.9 Comparison of chemical images and calculated percentage endosperm from 3BK material destined for reduction (left), cumulative break material to sizings (center), and reduction to tailings (right) for two millings. Note the additional endosperm from reduction to 3BK for the second milling and also the purity of sizings stock and tailings stock for the first milling.

3.3 Summary

The bottom line in flour milling production is the cumulative endosperm yield. This direct method for determining the part of the material that is endosperm and multiplying it by the quantity readily enables the quantitation of endosperm. This enables an experimentalist to calculate the mass balance for individual or successive unit processes with respect to the product exclusively. The ability to determine percentage endosperm by direct analysis of the solid mixture of chemical images allows the miller to determine the product (flour) yield rather than the presence of non-endosperm or inorganic residue.

Among the 1BK/2BK roll gap combinations in this experiment, the pair that provided the best recovery of endosperm was set at 0.022 in. (0.559 mm) for 1BK and 0.014 in. (0.356 mm) for 2BK. The 1BK/2BK roll gap combination of 0.024/ 0.014 in. (0.610/0.356 mm) resulted in the poorest endosperm recovery. The proportion of endosperm per unit of material extracted from the break system was 0.92 and 0.83 for the optimal and suboptimal combination, respectively. With the more aggressive combination, the total flour produced was higher; however, as might be expected, the non-endosperm fraction also increased. This experiment

shows the importance of continuous potential on-line optimization of break release settings in the mill when wheat mixes or any other variables affecting wheat performance change and is an additional step toward development of an effective on-line method for flour milling analysis.

Part 4: Application of Near Infrared Focal Plane Array Chemical Imaging to Feed Formulation Mixing Uniformity

4.0 Introduction

In the formulated feed industry, various ground, solid commodities are combined and blended prior to additional processing. Ribbon or paddle mixers are often used to blend the ingredients as they flow through the piece of equipment. The key is balancing uniformity of the blend with the cost of energy consumption for an adequate residence time. Lengthy mixing may also result in overmixing, which may potentially result in the reversal of mixing and segregation of materials. Key operational parameters to control in the mixing of solids include the revolutions per minute of the shaft, residence time, and ingredient feed rates. Once these operational parameters are optimized, future operation with the same product can be repeated before pelleting or extrusion cooking (45).

The uniformity of a formula feed commodity mixture is routinely monitored by use of a tracer. Many tracers used in the feed industry have the common flaw of differing by density, shape, or flow characteristics, from the granular commodities in a formulation (46). These include rock salt (47), which has differing flow characteristics from traditional commodities, and polymer beads that constitute a foreign substance. The ideal tracer would be an edible substance that would not effect processing and have the same characteristics as the formulation.

The term formulation used in the feed industry describes the ingredients and the characteristics which affect pellet quality including pellet ability, fiber, protein, and fat (48). Feed formulations start with a bulk commodity, such as ground maize or sorghum, the choice often depending on cost or availability. A protein supplement such as soybean meal, fish meal,

meat and bone meal, or blood meal is then used to meet guaranteed protein levels. The remainder of the ingredients consist of various minerals and organic micronutrients to serve different purposes.

Significant spectroscopic differences have been observed in the near IR region of the spectrum between protein supplements and base material in formulations (49). As such, protein supplements have the potential to serve as effective self-tracers of feed commodity mixtures if used at the same percentage the formulation specifies. Two tracer experiments were performed to determine mixing uniformity of a protein supplement/corn meal mixture (50). The first experiment used 48% protein soybean meal, a common and relatively available protein supplement. Blood meal, which has a distinct spectrum allowing selectivity among other protein supplements, was used as the tracer for the second experiment. Mixing uniformity was determined by comparing samples taken along a ribbon mixer shaft after a certain amount of ribbon shaft rotation cycles. Optimum mixing was considered to be achieved after the standard deviation reached a minimal steady state.

4.1 Experimental

4.1.1 Instrumentation

The Sapphire™ model indium InSb FPA (Malvern Instruments, Columbia, MD) imaging system was used for the imaging of granular feed mixtures as previously described in Part 3.2.1. The lens used produced a 13 mm x 10 mm FOV resulting in a 40 μm calculated pixel size. Spectral measurements were coadded over a period of 4 minutes. Three FOVs were averaged for each specimen to avoid localized sample differences.

4.1.2 Specimens and Procedure

Two tracer experiments were performed to test the potential of near IR imaging for feed mixing. Previous experimentation in our laboratory (49) has shown that significant differences between the near IR spectra of protein supplements enable single wavelength or multivariate distinction (Figure 4.1). The laboratory ribbon mixer **(**Wenger, Sabetha, KS**)** used was 66 cm

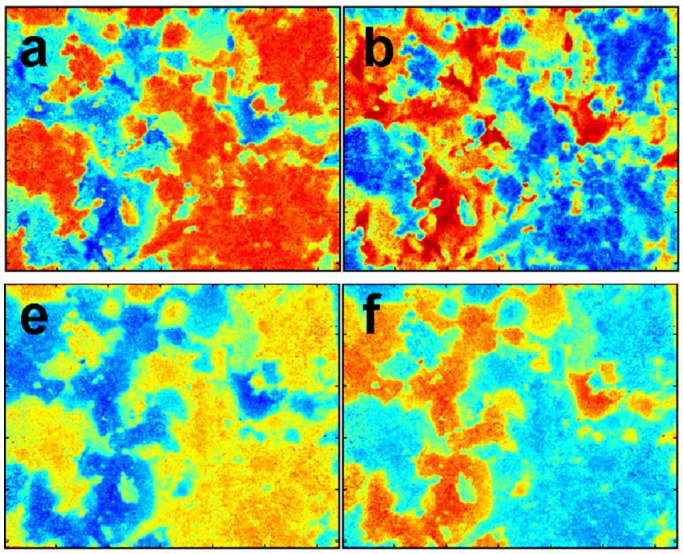

Figure 4.1 Contrasting single wavelength images for the same FOV highlighting (a) ground corn meal and (b) soybean meal with warm (red) false colors, of a 50/50 corn meal/soybean meal mixture. This was accomplished by using a starch band (2100 nm) and a protein band (1740 nm), respectively. Partial least squares (PLS) contrast highlighting (c) ground corn and (d) soybean meal is also shown for the same FOV. [Reprinted from 50]

long and equipped with a two cycle ribbon. Before mixing, corn meal was evenly spread out along the ribbon shaft. The respective tracer was then placed at the head of the mixer. For both experiments, sampling was accomplished by stopping the mixer at five cycle intervals and taking grab samples from four equally spaced intervals along the ribbon shaft. A preliminary set of grab samples was taken after a one cycle operation to show the early lack of uniformity. Spectra were collected for each sample in triplicate in the range of 1200–2400 nm and converted to absorbance. For the soybean meal tracer experiment, the wavelength segment 1851–1999 nm

was removed to eliminate the major near IR water band centered at 1940 nm. The experiment with the selective blood meal tracer (Figure 4.2) was limited to the wavelength range of 1200-

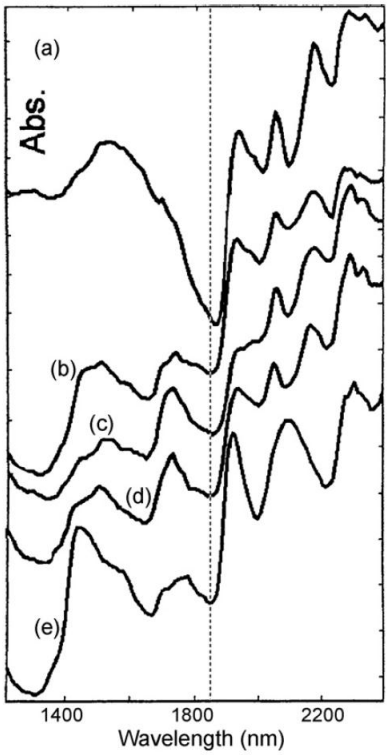

Figure 4.2 Representative near IR spectra of typical feed protein supplements (a) blood meal, (b) soybean meal, (c) fish meal, and (d) meat and bone meal. The spectrum of (e) corn meal is also shown for comparison. Note the unique spectrum of blood meal to the left of the 1850 nm demarcation. [Reprinted from 50]

1850 nm. The spectra were then baseline corrected and normalized. Prior to quantitation, two spectral libraries were acquired, one for soybean meal and corn meal and another for blood meal and corn meal. Each spectral library was based on approximately 164,000 pixels from each of the two component standards. The libraries allowed subsequent PLS characterization of each pixel in the binary mixtures. An algorithm was subsequently used to establish the percent of A (tracer) in a mixture of A and B (corn meal).

4.2 Results and Discussion

Figure 4.3 shows pairs of the triplicate images most representative of the average,

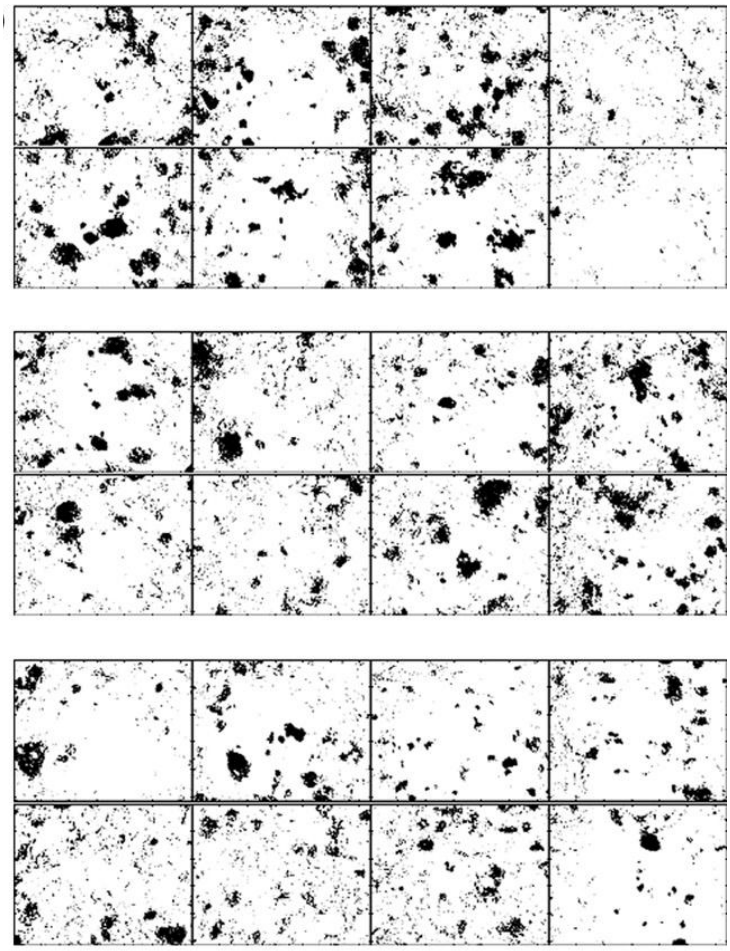

Figure 4.3 Each pair of four images (left to right) shows the population of soybean meal tracer along the ribbon shaft. The pairs are representative of the initial mixing (top), partial mixing at 15 cycles (middle), and a well-mixed sample after 25 cycles (bottom). A binary color scheme is used to highlight the soybean meal tracer. [Reprinted from 50]

concentration from the four positions along the shaft (head to tail, left to right) from the number of revolution cycles indicated for the soybean meal tracer experiment. Table III displays the

Table III Average of triplicate soybean meal percentages at each location along the ribbon shaft.

	A	B	C	D
Initial	23.1%	22.6%	26.8%	6.8%
5 cycles	14.2%	14.8%	12.1%	19.0%
10 cycles	16.0%	16.0%	13.1%	24.4%
15 cycles	17.4%	18.6%	19.6%	19.7%
20 cycles	13.6%	15.1%	13.6%	15.3%
25 cycles	15.7%	12.9%	14.8%	14.7%

[Reprinted from 50]

percentage soybean meal for each number of ribbon shaft revolution cycles for each position along the ribbon shaft. The relative standard deviation of the summation of each replicate for the four positions on the ribbon shaft was plotted as a function of the number of revolution cycles in Figure 4.4. The deviation dropped off dramatically after the initial mixing, but showed a slight

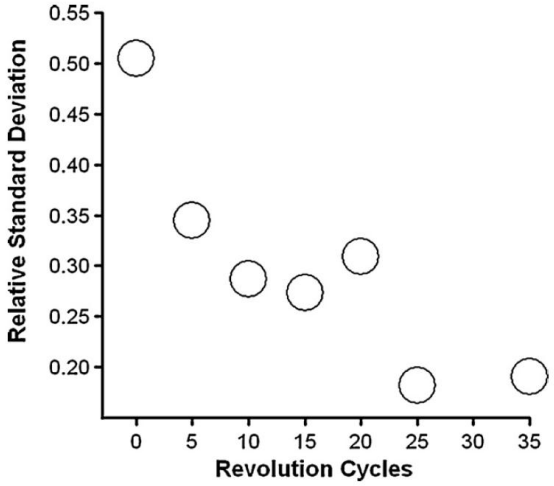

Figure 4.4 Precision as a function of mixing cycles is displayed for each triplicate image at each of the four locations along the ribbon shaft for the soybean meal/corn meal mixture. [Reprinted from 50]

decrease afterwards, until leveling off after 35 cycles. The elevated protein to starch ratio of soybean meal enabled excellent detection of soybean meal pixels in a binary mixture with corn meal in Figure 4.3.

The corresponding imaging results for the blood meal tracer are shown in Figure 4.5 and Table IV. A large skew in the percentage blood meal was observed for all samples, due in part to

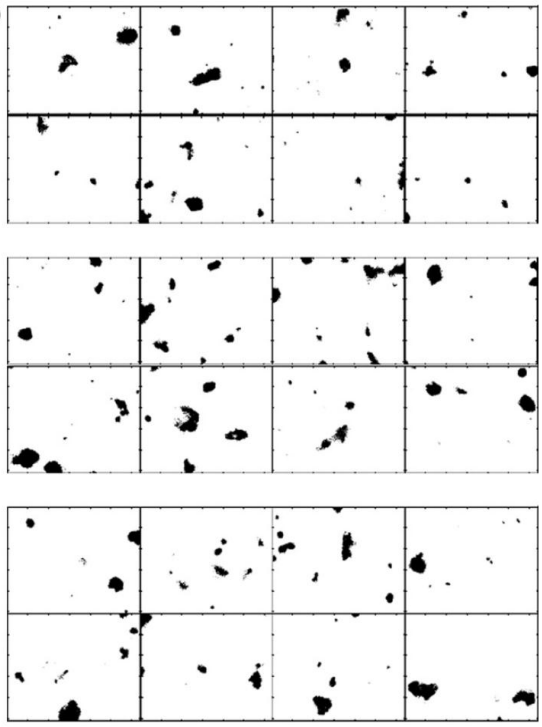

Figure 4.5 Each pair of four images (left to right) shows the population of blood meal tracer along the ribbon shaft. The pairs are from before mixing at 5 cycles (top), partial mixing at 15 cycles (middle), and a well-mixed sample after 25 cycles (bottom). A binary color scheme is used to highlight the blood meal tracer. [Reprinted from 50]

Table IV Average of triplicate blood meal percentages at each location along the ribbon shaft.

	A	B	C	D
Initial	–	–	–	–
5 cycles	32.9%	40.7%	13.5%	19.4%
10 cycles	–	–	–	–
15 cycles	31.9%	31.8%	41.7%	37.4%
20 cycles	–	–	–	–
25 cycles	34.9%	27.6%	45.1%	42.6%
90 cycles	–	–	–	–

[Reprinted from 50]

the strong intensity of blood meal in the selected wavelength range. In the presence of other tracers blood meal showed the greatest selectivity as a tracer. A well-mixed portion of the blood meal/corn meal mixture was diluted with soybean meal to produce a 73.6%:20.0%:6.4% (by weight) corn meal/soybean meal/blood meal mixture. The blood meal/corn meal PLS characterization was then applied to the mixture. The measured percentage blood meal for these samples was diminished due to the dilution, but there was no misidentification of soybean meal pixels as blood meal.

4.3 Summary

While NIR quantitative imaging of heterogeneous commodity mixers may require replication, both commodity tracers showed distinct advantages for accurate studies of feed mixing uniformity. Soybean meal, as a commonly used protein supplement, would show flexibility for a variety of feed formulations. Blood meal unique spectroscopic features among other protein supplements would allow its inclusion at low levels in feed formulations. The decreased NIR range used for the blood meal study also shows the potential for a simplified calibration and online analysis. Both commodity tracers provide the same advantage of matching the flow characteristics of the bulk material. However, the sampling procedures described here would not be ideal in an industrial environment with moving product. Testing would be accomplished by taking samples from the output of the mixer. Uniformity of the feed commodity mixtures would be determined by calculating the time necessary for minimization of the standard deviation between multiple samples or predetermining the measured amount of tracer in an ideally mixed formulation and obtaining that value. Relative heterogeneity found along the mixer ribbon shaft for even the well-mixed material was evident in this experiment, as proved by a

measure 8.6% RSD for a 60%:40% soybean meal/corn meal mixture. Sampling from the end of the mixing unit would ideally improve the representativeness of the samples measured.

Part 5: Summary

Chemical imaging was successful for the microspectroscopic study of modification within single starch granules and the near IR differentiation of starch between another component of a binary mixture for both flour milling and feed milling. The combination of a multi-beam synchrotron source and FPA detection at the IRENI beamline allows for fast acquisition of imaging data with approximately 0.54 μm resolution approaching the diffraction limit. The comparison between data from previous confocal synchrotron IMS and the current state-of-the-art IRENI data showed greater heterogeneity of localized ester carbonyl modification within granules for FPA synchrotron IMS.

Near infrared FPA instrumentation allows significant flexibility for the analysis of solid mixtures of flour and feed milling products. Specific regions of the near IR spectrum or specific wavelength combinations can be utilized for informed analyses. However, the high capital cost of the FPA instrumentation and software does not make sense in the case of low-margin industries. This instrumentation could make sense for companies with central laboratories where samples can be sent in and analyzed could be reasonable, particularly for the optimization of unit process. Additionally, further work is trending towards the potential of on-line near infrared quantitation for milling applications. The potential of future method development is greatly enhanced by the flexibility of the FPA near IR imaging.

References

1. Wetzel, D.L and Levine, S.M. 1999. Microspectroscopy: imaging molecular chemistry with infrared microscopy. *Science*. 285(5431): 1224-1225.

2. Budevska, B.O. 2002. Vibrational spectroscopy imaging of agricultural products. In: *Handbook of Vibrational Spectroscopy*. J.M. Chalmers and P.R. Griffiths (eds.) John Wiley & Sons Ltd: Chichester, Vol.1, Pgs. 3720-3732.

3. Kwiatkoski, J.M. and Reffner, J.A. 1987. FTIR microspectrometry advances. *Nature* 328(27),:837-838.

4. Griffths, P.R. and deHaseth, J.A. 1986. The Michelson interferometer. In: *Fourier Transform infrared spectrometry*. John Wiley & Sons Ltd: New York.

5. Carr, G.L., Reffner, J.A., and Williams, G.P. Performance of an infrared microspectrometer at the NSLS. *Rev. Sci. Instr.*, 66:1490-1492.

6. Jamin, N., Dumas, P., Moncuit, J., Fridman, W.H., Teilland, J.L., Carr, G.L. and Williams, P.G. 1998. Highly resolved chemical imaging of living cells by using synchrotron infrared microspectrometry. *Proc. Natl. Acad. Sci. U.S.A.* 95:4837.

7. Jamin, N., Dumas, P., Moncuit, J., Fridman, W.H., Teilland, J.L., Carr, G.L. and Williams, P.G. 1998. Chemical imaging of nucleic acids, proteins and lipids of a single living cell. Application of synchrotron infrared microspectrometry in cell biology, *Cell Mol. Biol.* 44:9.

8. Dumas, P. 2005. Synchrotron IR experiments: from microanalysis to pump–probe experiments. In: Proceedings of the 56th Annual Pittsburgh Conference on Analytical Chemistry and Applied Spectroscopy, Orlando, FL.

9. Lewis, E.N., Treado, P.J., Reeder. R.C., Story, G.M., Dowrey, A.E., Marcott, C., Levin, I.W. 1995. Fourier Transform spectroscopic imaging using an infrared focal plane array detector. *Anal. Chem.* 67:3377-3381.

10. Marcott, C., Reeder, R.C., Sweat, J.A., Panzer, D.D. and Wetzel, D.L. 1999. FTIR Spectroscopic imaging microscopy of wheat kernels using a Mercury Cadmium Telluride focal plane array detector. *Vibr. Spectrosc.* 19:123-129.

11. Carr, G.L. 2001. Resolution limits for infrared microspectroscopy explored with synchrotron radiation. *Rev. Sci. Instr.* 72:1613.

12. Moss, D., Gasharova, B. and Mathis Y.-L. 2006. Practical tests of a focal plane array detector microscope at the ANKA-IR beamline, *Infrared Phys. Tech.* 49(no. 1-2):53-56.

13. Miller, L.M. and Dumas, P. 2006. Chemical imaging of biological tissue with synchrotron infrared light. *Biochim. Biophys. Acta Biomembranes* 1758*(*7):846-857.

14. Walsh, M.J., Nasse, M.J., Pounder, F.N., Macias, V., Kajdacsy-Balla, A., Hirschmugl, C.J. and Bhargava, R. Synchrotron FTIR imaging for the identification of cell types within human tissues. *AIP Conf. Proc.* 12-14:105.

15. Kaye, W. 1954. Near-infrared spectroscopy: I. Spectral identification and analytical applications *Spectrochim. Acta* 6:257-287.

16. Kaye, W. 1955. Near-infrared spectroscopy II. Instrumentation and technique, *Spectrochim. Acta* 1:181-204.

17. Wetzel, D.L. 1983. Near-infrared reflectance analysis: Sleeper among spectroscopic techniques, *Anal. Chem.* 55:1165A-1176A.

18. McClure, W.F. and Stanfield, D.L. 2002. Near infrared spectroscopy of biomaterials. In: *Handbook of Vibrational Spectroscopy*. J.M. Chalmers and P.R. Griffiths (eds.) John Wiley & Sons Ltd: Chichester, Vol.1.

19. Smail, V.W., Fritz, A.K. and Wetzel, D.L. 2006. Chemical imaging of intact seeds with NIR focal assists plant breeding. *Vibr. Spectrosc*. 42:215–221.

20. Dubois, J., Lewis, E.N., Fry Jr., F.S. and Calvey, E.M. 2005. Bacterial identification by near infrared chemical imaging of food specific cards. *Food Microbiology*. *22*:577–583.

21. Wetzel, D. L., Posner, E. S. and Dogan, H. 2010. Indium antimonide (InSb) focal plane array chemical imaging enables assessment of unit process efficiency for milling operation. *Appl. Spectrosc.* 64(12):1320-1324.

22. Lee, E., Huang, W.X., Chen, P., Lewis, E.N. and Vivilecchia, RV. 2006. High throughput analysis of pharmaceutical tablet content uniformity by near infrared chemical imaging. *Spectrosc.* 21(11):24-32.

23. Dubois, J., Wolff, .J, Warrack, J.K, Schoppelelrei, J. and Lewis, E.N. 2007. NIR chemical imaging for counterfeit pharmaceutical products analysis. *Spectrosc.* 22(2):40-50.

24. BeMiller, J.N. 2007. In: *Carbohydrate Chemistry for Food Scientists, Second Edition*, American Association of Cereal Chemists, St. Paul, MN.

25. Swinkels, J.J.M. 1985. Composition and properties of commercial native starches, *Starch/Stärke* 37:1-5.

26. FDA. Code of Federal Regulations. Title 21, Chap. I, Part 172. 1994. Food Additives Permitted in Foods for Human Consumption, Section 172.892, Food Starch-Modified, U.S. Government Printing Office, Washington, DC.

27. Mathlouthi, M. and Koenig, J. 1986. Vibrational spectra of carbohydrates. *Adv. Carbohydr. Chem. Biochem.* 44:7–89.

28. Kacurakova M. and Wilson, R.H. 2001. Development in mid-infrared FT-IR spectroscopy of selected carbohydrates. *Carbohydr. Polym.* 44:291–303.

29. Fang, J., Fowler, P., Sayers, C. and Williams, P. 2004. The chemical modification of a range of starches under aqueous reaction conditions. *Carbohydr. Polym*. 55:283–289.

30. Chi, H., Xu, K., Xue, D.H., Song, C.L., Zhang, W.D. and Wang, P.X. 2007. Synthesis of dodecenyl succinic anhydride (DDSA) corn starch, *Food Res. Int.* 40:232–238.

31. Song, X., He, G., Ruan, H. and Chen, Q. 2006. Preparation and properties of octenyl succinic anhydride modified early Indica rice starch. *Starch/Stärke*. 58:109–117.

32. He, J., Liu, J. and Zhang, G. 2008. Slowly digestible waxy maize starch prepared by octenyl succinic anhydride esterification and heat moisture treatment: Glycemic response and mechanism. *Biomacromolecules.* 9:175–184.

33. Bai, Y., Shi, Y.-C. and Wetzel, D.L. 2009. Fourier transform infrared (FT-IR) microspectroscopic census of single starch granules for octenyl succinate ester modification. *J. Agric. Food Chem.* 57:6443.

34. Shi, Y.-C., Reffner, J.A. and Wetzel, D.L. 2010. Synchrotron infrared confocal microspectroscopical detection of heterogeneity within chemically modified single starch granules. *Appl. Spectrosc.* 64:282-285.

35. Nasse, M.J., Walsh, M.J., Mattson, E.C., Reininger, R., Kajdacsy-Balla, A., Macias, R.V., Bhargava, R. and Hirschmugl, C.J. 2011. High-resolution Fourier-transform infrared chemical imaging with multiple synchrotron beams, *Nat. Methods* 8(5):413-416.

36. Carr, G.L., Chubar, O. and Dumas, P. 2006. Multichannel detection with a synchrotron light source: design and potential, In: *Spectrochemical Analysis Using Infrared Detectors*. R. Bhargava (ed.). Blackwell Publishing. Pgs 56–84.

37. King, R.W. 1989. Physiology of sprouting resistance. In: *Preharvest Field Sprouting in Cereals.* N.F. Derera (ed.) CRC Press, Inc.: Boca Raton, Florida. Pg 2855.

38. Posner E.S. and Hibbs A.N. 2005. In: *Wheat Flour Milling, 2nd ed.* AACC: St. Paul, MN. Pgs 125-53.

39. Gwirtz, J.A. 2011. A new imaging method in milling. *World Grain.* October:76-80.

40. Gwirtz , J.A. 2012. New imaging method in milling. *Milling Journal*. 19(4):56-58.

41. Eliott, R. 1989. Specification flours – an alternative approach. *AOM Technical Bulletins*. March:5413-5414.

42. Jagger, J.C.G. 1990. Robinson milling systems – rollermill automation package. *AOM Technical Bulletins.* November:5786-5787.

43. Wingfield, J., 1989. Break release / Extraction survey – 1988, Compiled for the technical committee. *AOM Technical Bulletins*. March:5415-5422.

44. Li, Y.Z., and Posner, E.S., 1987. The influence of kernel size on wheat millability. *AOM Technical Bulletins*. November:5089-5095.

45. Altland, G. and Pfost, H.B. 1976. In: *Feed Manufacturing Technology,* American Feed Manufacturers Association, Arlington, VA.

46. Fogler, H.S. 1999. In: *Elements of Chemical Reaction Engineering, 3rd edition*. New Jersey: Prentice-Hall, Inc.

47. E.A. Salim, The effect of tracers' physical properties on retention time measurements inside the conditioner of a pellet mill, MS Thesis, Kansas State University, 2008.

48. MacBain, R. 1966. Pelleting Animal Feed. Regional feed school. Arlington, Va. American Feed Manufacturers Association.

49. Brewer, L.R., Charles, H.E. and Wetzel, D.L. 2009 Processed mixture analysis for ingredient identity, concentration, and distribution by near-IR focal plane array chemical imaging, In: 60th Annual Pittsburgh Conference on Analytical Chemistry and Applied Spectroscopy, paper no. 420-3.

50. Wetzel, D.L., Brewer, L.R., and Boatwright, M.D. 2010. Granular solid formulation commodity mixture uniformity revealed via InSb focal plane array chemical imaging, *Vib. Spectrosc.* 53(1):83-87.